

Submitted to *The Astrophysical Journal* on May 24, 2000

(revised: Sept. 14, 2000)

X-ray spectral features from GRBs: Predictions of progenitor models

Markus Böttcher*¹ and Chris L. Fryer^{†2}

*Space Physics and Astronomy Department; Rice University, MS 108
6100 S. Main Street; Houston, TX 77005 - 1892; USA

[†]Theoretical Astrophysics, Los Alamos National Laboratory; Los Alamos, NM 87545; USA

ABSTRACT

We investigate the potentially observable prompt or delayed X-ray spectral features from the currently popular gamma-ray burst (GRB) models. During the evolution of many GRB progenitors, a disk around the central GRB source is produced. Shock heating as the GRB ejecta collide with the disk may produce observable X-ray features. We first summarize predictions deduced from previous calculations which invoke photoionization and relativistic blast waves. We then calculate the quasi-thermal X-ray line features produced assuming the ejecta are nonrelativistic (which is more likely for the disk interactions of many GRB models). In the framework of the Hypernova/Collapsar model, delayed (a few days – several months after the GRB) bursts of line-dominated, thermal X-ray emission may be expected. The He-merger scenario predicts similar X-ray emission line bursts \lesssim a few days after the GRB. These X-ray signatures should be observable with *Chandra* and *XMM-Newton* out to at least $z \sim 1$. Weak emission line features \lesssim a few days after the GRB may also result from the supranova GRB scenario. In all three cases, significant X-ray absorption features, in particular during the prompt GRB phase, are expected. No significant X-ray spectral features should result from compact-object binary mergers.

Subject headings: supernovae: general — gamma-rays: bursts — X-rays: bursts

1. Introduction

With the advent of the new generation of X-ray telescopes, such as *Chandra* and *XMM-Newton*, the detection of X-ray spectral signatures from the environments of cosmological gamma-ray bursts (GRBs) has become a realistic prospect. The marginal detection of a redshifted Fe K α emission line in the afterglow of GRB 970508 (Piro et al. 1999) with the *BeppoSAX* NFI has stimulated a vital discussion about the possible

¹Chandra Fellow

²Feynman Fellow

origin of this line feature (Ghisellini et al. 1999; Lazzati et al. 1999; Böttcher et al. 1999a; Böttcher, Dermer, & Liang 1999b; Vietri et al. 1999; Weth et al. 2000; Paerels et al. 2000; Böttcher 2000). So far, this discussion has concentrated on determining the required / inferred physical conditions in the vicinity of GRB 970508 needed to explain the iron-line feature in the afterglow (assuming this feature is real).

An essential assumption in these papers was that the material responsible for potential emission line features is illuminated (and partially or completely ionized) by burst emission which is qualitatively similar to the observed GRB and afterglow radiation. Also, these papers assume that the blast wave which interacts with the line-emitting material is relativistic, and qualitatively similar to the one which is associated with the GRB and its afterglow. The conditions inferred under these assumptions are rather extreme, requiring large amounts ($\sim 10^{-4} M_{\odot}$) of iron to be concentrated anisotropically in a small ($R \lesssim 10^{-3}$ pc) region around the central engine of the GRB (e.g., Lazzati et al. 1999, Weth et al. 2000, Böttcher 2000). Paerels et al. (2000) have recently suggested that high-resolution X-ray spectroscopy may help to distinguish between different line production mechanisms as a way to unveil the underlying physical scenario. They argue that, in particular, photoionization can be distinguished from collisional excitation of the line by virtue of the lower plasma temperature resulting in photoionization scenarios. In their detailed analysis of the BeppoSAX MECS spectrum of GRB 970508 during the time segment in which the ~ 3.6 keV emission line was marginally detected, they found that the line width and apparent strength of the radiative recombination continuum blueward of the emission line, in combination with the measured redshift of the GRB at $z = 0.835$, are inconsistent with a photoionization scenario in which the source of the line emission is in photoionization equilibrium with the afterglow radiation.

In addition to this evidence, most of the currently popular gamma-ray burst models may be hard-pressed to produce the conditions inferred from photoionization-based scenarios to explain the observed iron-line feature in GRB 970508. These models are not ruled out, both because the iron line feature in GRB 970508 is marginal, and even if it is real, it may appear only in one small subclass of GRBs. However, Vietri et al. (1999) have used this line to argue for their alternative supranova model (Stella & Vietri 1998) which invokes the collapse of a neutron star as it spins down. Unfortunately for this model, realistic calculations of collapsing neutron stars (Ruffert, Janka, & Schäfer 1996; Fryer & Woosley 1998) find that these collapses eject too much baryonic material and have too little energy to produce GRBs. Because these models do not include magnetic fields, this does not rule out the supranova model. Even so, the supranova model would most likely produce a short burst, and hence can not explain the line feature seen in GRB 970508, since that burst was a long-duration burst with $t_{\gamma} \sim 25$ s.

Instead of trying to explain GRB 970508, in this paper we look at the more viable “black-hole accretion disk” class of GRB engines (see Fryer, Woosley, & Hartmann 1999 for a review) and estimate potential X-ray spectral features in GRB afterglows that these models produce. We make the initial assumption that these features are produced by the collision of the GRB ejecta with the environment produced during the formation process of the GRB engine. In the Collapsar and he-merger engines, the GRB is surrounded by a disk of material which is produced during their progenitor evolution. MacFadyen & Woosley (1999) found that collapsar (and probably he-merger) GRBs are beamed, forming a jet along the angular momentum axis of the accreting disk. They also found that the explosion along the equator is likely to be very baryon loaded ($>1 M_{\odot}$) moving at velocities much less than the speed of light (less than $\sim 10^9$ cm s $^{-1}$). In §2, we discuss the formation of these nonrelativistic disks around black-hole accretion disk GRBs, estimating the structure of each disk. We then use these structures in §§3 and 4 to predict the X-ray afterglow signature of these GRBs. We conclude with a discussion of the implications these results have on current and future X-ray missions in §5.

We note that the predictions concerning potentially time-variable absorption features as derived by Ghisellini et al. (1999) and Böttcher et al. (1999a) are valid, independent of the detailed GRB mechanism. Obviously, material responsible for such X-ray absorption features is located along the line of sight to the burst, so that the observed GRB and afterglow radiation and the assumption of a relativistic blast wave may be used.

2. Disk formation

Nearly all of the formation scenarios of black hole accretion disk GRBs invoke a “common-envelope” phase. Binaries are said to be in a common-envelope phase when the hydrogen envelope of one star engulfs its companion (this usually occurs when the star expands into a giant or supergiant). Friction and/or tidal forces cause the companion to spiral in towards the giant’s helium core, ejecting the hydrogen envelope. The evolution of two stars that enter a common envelope phase is one of the major uncertainties in binary population synthesis and, despite years of effort, still remains an open question (see Sandquist et al. 1998 and references therein). This limits our ability to make any strong quantitative predictions of this phase, but we can use the latest simulations to guide our estimates. Current simulations (e.g. Sandquist et al. 1998) suggest that the companion inspiral occurs on a timescale of 1 – 10 orbital periods (t_{orbit}). The outcome of this inspiral is either: a) a close binary system if the companion is able to eject the hydrogen envelope before it merges with the star’s helium core or b) a merged object if the stars merge before the ejection of the hydrogen envelope.

The hydrogen envelope carries away much of the orbital angular momentum and is preferentially ejected in the orbital plane (Sandquist et al. 1998). It is this material which forms the disks around GRB engines. Double NS, BH-NS, and BH-WD mergers go through a common envelope phase long before they actually merge, and the progenitors of these GRBs travel far from their formation sites (and their common-envelope disks) before producing GRBs (e.g. Fryer et al. 1999, Bulik & Belczyński 1999 and references therein). Collapsar and he-merger GRBs, on the other hand, occur shortly after their common-envelope phase. In this paper, we study the interaction of the ejecta from the GRB explosion with the common-envelope disks produced by collapsar and he-merger progenitors and determine the spectral features of this interaction. But first we must estimate the structure and size of these disks.

2.1. He-merger disks

To understand the characteristics of the disks produced in he-mergers, we must first understand the formation process of he-mergers (for more details, see Fryer et al. 1999). The progenitor of a he-merger GRB is a binary system with two massive stars (both stars have masses in excess of $\sim 8 M_{\odot}$). The more-massive star (primary) evolves through its life, collapsing to form a compact remnant (either a neutron star or black hole). During the initial expansion, the primary may transfer mass to its companion (secondary star), and this mass transfer (or even a common-envelope phase) may tighten the orbital separation of these binaries. For some binaries, asymmetries in the primary’s supernova explosion also lead to a tighter binary system as the compact remnant is “kicked” into a closer orbit with its companion. In addition, the ejecta from the supernova explosion may enrich the envelope of the secondary (see Israelian et al. 1999) with r-process elements.

When the secondary evolves off the main sequence, it envelops the primary’s compact remnant, and

the binary goes into a common-envelope phase. The compact remnant ejects the hydrogen envelope in a disk-like structure, but not before merging with the secondary’s helium core. A he-merger occurs after the compact remnant has settled into the helium core. The inspiral process spins up the helium core, producing a disk around the compact remnant. In addition, the compact remnant accretes $\sim 1 - 3 M_{\odot}$ during the inspiral and disk formation process (Zhang & Fryer 2000), causing it to collapse to a black hole if it is not one already. This black-hole accretion disk system is surrounded by a disk formed from the enriched hydrogen envelope of the secondary.

There are no simulations of the common-envelope evolution of a compact remnant into a massive star which reliably predict the ejecta from the inspiral process. However, we may extrapolate from simulations such as Sandquist et al. (1998) to obtain a rough estimate of the characteristics of the hydrogen disk. The ejection velocity (v_{ejection}) is roughly the escape velocity at any given radius in the star:

$$v_{\text{ejection}} = \sqrt{\frac{2GM(r)_{\text{secondary}}}{r}}. \quad (1)$$

The time between GRB outburst and the ejection of matter is equal to the inspiral time (since the outburst occurs as soon as the neutron star spirals into the center of the secondary):

$$t_{\text{GRB}} \approx 10t_{\text{orbit}} = \frac{20\pi r^{1.5}}{G^{0.5}M(r)_{\text{secondary}}^{0.5}}. \quad (2)$$

At the time of the GRB outburst, the location of any layer of star with radius r is simply:

$$D_{\text{ejecta}} \approx v_{\text{ejection}} \times t_{\text{GRB}} = 20\sqrt{2}\pi r. \quad (3)$$

Clearly, the density structure of any he-merger disk depends upon the density structure of the secondary at the start of the common envelope phase. This structure is a function of both the size of the star (and hence, the orbital separation of the binary) at the beginning of the common-envelope phase and the mass distribution of the companion star. Using the binary population synthesis code developed in Fryer et al. (1999), we can calculate the distribution of orbital separations and companion masses for he-merger progenitors (Figs. 1 and 2). Fig. 3 shows the range of hydrogen disk structures formed by he-mergers with a $15 M_{\odot}$ companion star for a series of orbital separations. Note that the outer disk radius is most sensitive to the orbital separation prior to the common envelope evolution. Fig. 4 shows the range of disk structures formed by 15, 25, and $40 M_{\odot}$ stars assuming the orbital separation is set to the maximum radius of the companion. Although our rough estimates of the disk formation and the uncertainties in binary population synthesis and stellar evolution (see Fryer et al. 1999 for a discussion) make it difficult to predict the density profile of these disks accurately, these figures give a flavor of the range of possible disk structures.

2.2. Collapsar disks

The ring around Supernova 1987A proves that at least some massive stars have disks. The progenitor of Supernova 1987A was probably a binary system in which the more massive primary engulfed its companion, causing the companion to spiral into the primary during a common-envelope phase (Podsiadlowski 1992). The companion was unable to eject the entire hydrogen envelope and it merged with the primary’s helium core. This process could lead to the formation of an outward moving disk which, in the case of supernova 1987A, was lit up 10,000 – 100,000 years later by the supernova to reveal a “ring” (see for example, Collins et al. 1999).

The majority of Collapsar progenitors also follow an evolutionary path where a binary system goes through a common envelope phase although the companion often does not merge with the primary (Fryer et al. 1999). The “classical” Collapsar model requires a massive helium star (without a hydrogen envelope) to avoid baryon contamination (MacFadyen & Woosley 1999), and a common-envelope phase is required to eject most of the hydrogen envelope (Fryer et al. 1999). Unlike the he-merger disks, the common envelope phase can occur more than 100,000 years before the eventual GRB outburst. Although the Collapsar progenitor is still likely to be surrounded by this ejecta, disks formed in Collapsar progenitors will be much further away at outburst than those disks formed in he-mergers. Assuming an ejection velocity equal to the escape velocity (eq. 1) and setting the time from disk ejection to GRB outburst (t_{GRB}) to 100,000 y, we find that the inner edge of most Collapsar disks exceeds 10^{17} cm.

However, if the binary does not go into a common-envelope until just before the collapse of the primary, a much more compact disk may be formed. Recall that a common-envelope phase occurs when the radius of a star expands enough to engulf its companion. Most stellar models reveal that a star actually contracts during the last 10,000 – 100,000 y of its life (Schaerer et al. 1993, Woosley & Weaver 1995). If the binary does not enter a common-envelope phase before this contraction, it is unlikely that it ever will. So with the current stellar models, t_{GRB} must be greater than 10,000 – 100,000 y. However, stellar models do not accurately predict the radii of massive stars, and there is a growing concern that these radii may be drastically incorrect (Fryer et al. 1999, Wellstein & Langer 1999, Fryer & Kalogera 2000). It is possible that massive stars reach their maximum size just before collapse. If the common-envelope phase occurs 10 – 100 years before collapse, the inner edge of the disk could be less than 10^{15} cm. Until accurate stellar models are produced, we can not refine our estimates further. However, even with these rough estimates of the disk structure, we can now estimate the expected X-ray afterglow spectral features from both of these objects.

X-rays may also be produced when the GRB ejecta strikes the Collapsar’s companion star. Recall that the companion generally does not merge with the collapsar during the common envelope phase. The ejecta will hit this companion star, causing it to heat and expand, producing an X-ray emitting nebula (P. Pinto - private communication). The magnitude and spectra of X-rays under this mechanism is difficult to predict quantitatively, and we will delay further discussion of this emission for a later paper.

3. Predicted X-ray spectral features

3.1. Analytic estimate of the maximum iron line luminosity

In this section, we present a simple analytic estimate for an upper limit to the total, isotropic luminosity in the two major constituents of the iron $K\alpha$ line blend from a hot, highly ionized plasma, namely the Fe XXV $\text{He}\alpha$ ($2p1s \rightarrow 1s^2$ resonance) and the Fe XXVI $\text{H}\alpha$ ($2p \rightarrow 1s$) transitions. Apart from energy conservation constraints, the luminosity in the resonant emission lines considered here is restricted by several line destruction mechanisms, such as Compton scattering, photoelectric absorption by lighter elements, and collisional de-excitation. Considering Compton scattering and photoelectric absorption — both of which processes would remove a line photon from the line — one can define an effectively emitting volume given by the fraction of the total disk volume through which the optical depth $\tau_L \equiv \tau_T + \tau_{\text{pa}} \equiv \tau_T (1 + f_{\text{pa}})$ due to electron scattering and photoelectric absorption is ~ 1 . In a neutral plasma of cosmic element abundance, we have $f_{\text{pa}} \sim 4$ at the energies of the $n = 2 \rightarrow 1$ transitions of Fe XXV and Fe XXVI. In an ionized plasma, this number obviously becomes smaller, and for our simple estimate we assume $f_{\text{pa}} \sim 2$. The effect of collisional de-excitation becomes relevant if the density of the line-emitting material becomes comparable

to or greater than the critical density n_{crit} at which the collisional de-excitation rate equals the spontaneous decay rate. Using van Regemorter’s (van Regemorter 1962) \bar{g} approximation, the critical density can be roughly approximated as

$$n_{\text{crit}}^{\text{c.d.}} \approx 2.4 \times 10^{11} \frac{\sqrt{T_e/\text{K}}}{\lambda_{\text{nm}}^3} \text{ cm}^{-3} \approx 3.8 \times 10^{17} T_8^{1/2} \text{ cm}^{-3}, \quad (4)$$

where $T_8 = T/(10^8 \text{ K})$.

For the ease of computation, we assume that the emitting region can be geometrically represented by a torus, located at a distance $r = 10^{13} r_{13}$ cm from the center of the burst source, with a cross-sectional radius of $a = 10^{12} a_{12}$ cm, containing a total mass of $M_{\text{T}} = m_{\text{T}} M_{\odot}$, the volume of the torus will be given by $V_{\text{T}} = 2 \times 10^{38} a_{12}^2 r_{13} \text{ cm}^3$. The average density of the torus material is then $n_{\text{T}} = 6 \times 10^{18} [m_{\text{T}}/(a_{12}^2 r_{13})] \text{ cm}^{-3}$. If the observer is looking along a line of sight close to the symmetry axis of the torus, then the Thomson depth through the torus is reasonably well approximated by

$$\tau_{\text{T}} = a n_{\text{T}} \sigma_{\text{T}} = 4 \times 10^6 \left(\frac{m_{\text{T}}}{a_{12} r_{13}} \right). \quad (5)$$

We define a critical density for Thomson scattering, $n_{\text{crit}}^{\text{T}}$ as the density at which the Thomson depth equals 1, so that for densities $n > n_{\text{crit}}^{\text{T}}$ line photons are likely to be scattered out of the line before leaving the emitting volume. This critical density is given by $n_{\text{crit}}^{\text{T}} \approx 1.5 \cdot 10^{12} a_{12}^{-1} \text{ cm}^{-3}$. In the situations of interest here, we always find $n_{\text{crit}}^{\text{T}} \ll n_{\text{crit}}^{\text{c.d.}}$, indicating that line destruction by Compton scattering and photoelectric absorption is dominant over collisional de-excitation.

The luminosity in the emission lines may thus be estimated as $L_{\text{line}} = j_{\text{L}} V_{\text{T}} / \max\{\tau_{\text{L}}, 1\}$, where j_{L} is the emissivity in the line. In order to parametrize the line emissivities by an emissivity parameter x , we use the notation of Raymond & Smith (1977), where $j_{\text{L}} = n_{\text{H}} n_{\text{e}} \cdot 10^{-23-x} \text{ erg cm}^{-3} \text{ s}^{-1}$. The emissivity parameters are inferred from runs of the XSTAR code (Kallman & McCray 1982) with a negligibly small ionization parameter of $\xi = 10^{-8} \text{ ergs cm s}^{-1}$ and constant, pre-specified plasma temperature. This yields

$$L_{\text{line}} \approx 6 \cdot 10^{45-x} \frac{m_{\text{T}}}{a_{12}} \text{ ergs s}^{-1}. \quad (6)$$

Some representative values of the emissivity parameters x and the upper limits on the line luminosities are listed in Table 1, and the estimated luminosity upper limits are plotted as a function of plasma temperature in Fig. 5. Although these are very crude estimates, they indicate that Fe $K\alpha$ luminosities in excess of $\sim 10^{44} \text{ ergs s}^{-1}$ are very well possible in a shock-heated-disk scenario.

3.2. Simulations of the shockwave / disk interaction

In order to get a realistic prediction of the expected X-ray line and continuum emission from the shock-heated disk, we simulate the shock-wave evolution and thermal history of the shocked material as the supernova ejecta, associated with the GRB explosion, interact with the pre-ejected disk. We assume that in the course of the supernova/GRB a total mass of $M_0 \sim 1 M_{\odot}$ is ejected quasi-isotropically at a speed of $v_s = 10^9 v_9 \text{ cm s}^{-1}$, initiating a shock-wave when interacting with the disk of pre-ejected material.

For the case of an intermediate-mass (secondary) progenitor (15, 25 M_\odot), we parametrize the density profile of the disk by $\rho_d(r) = \rho_0 (r/r_{\text{in}})^{-2.5}$ for $r_{\text{in}} \leq r \leq r_{\text{out}}$ and its geometry by a constant $h/r \sim 0.1$. For more massive stars (40 M_\odot) the density profile may be approximated by a broken power-law with $\rho_d(r) = \rho_0 (r/r_{\text{in}})^{-4}$ for $r_{\text{in}} \leq r \leq r_{\text{br}}$, and $\rho_d(r) = \rho_0 (r_{\text{br}}/r_{\text{in}})^{-4} (r/r_{\text{br}})^{-1}$ for $r_{\text{br}} \leq r \leq r_{\text{out}}$ (see Fig. 4). Writing $r_{\text{in}} = 10^x r_{i,x}$ cm and $n_0 = \rho_0/(\bar{A} m_p) = 10^{17} n_{17}$ cm $^{-3}$, where \bar{A} is the average atomic weight of the disk material, the total mass in the pre-ejected disk is

$$M_d = 0.1 \left(\frac{h/r}{0.1} \right) n_{17} r_{i,13}^3 \left(\sqrt{\frac{r_{\text{out}}}{r_{\text{in}}}} - 1 \right) M_\odot \quad (7)$$

for intermediate-mass progenitors, and

$$M_d = 0.5 \left(\frac{h/r}{0.1} \right) n_{21} r_{i,12}^3 \left(1 + \frac{r_{\text{in}} r_{\text{out}}^2}{2 r_{\text{br}}^3} \right) M_\odot \quad (8)$$

for high-mass progenitors.

The deceleration of the non-relativistic shock wave and the heating of the ejecta and the swept-up material, are calculated by numerically solving simultaneously for the energy and momentum equations,

$$\frac{d}{dt} (M v_s) = 4\pi R_s^2 \bar{P}_s, \quad (9)$$

$$\frac{dM}{dt} = 4\pi R_s^2 \rho_d(R_s) v_s, \quad (10)$$

$$\frac{dE}{dt} = -\bar{P}_s \frac{dV}{dt} + \dot{E}_{\text{rad}}, \quad (11)$$

where

$$E = \frac{1}{2} \bar{\rho}_s v_s^2 V + \frac{\bar{P}_s V}{\gamma - 1}, \quad (12)$$

R_s is the shock radius, \bar{P}_s and $\bar{\rho}_s$ are the volume-averaged pressure and density of the shocked material, V is the volume occupied by the shocked material, γ is its adiabatic index, and \dot{E}_{rad} is the radiative cooling term. Throughout this paper, we assume $\gamma = 5/3$. In Eq. 9, we have neglected the pressure of the disk material.

Due to the high densities involved and to the fact that the shock wave is non-relativistic, we may assume that at any point in time the shocked material is in approximate thermal and collisional ionization equilibrium. Photoionization precursors are not expected to play an important role since the Compton scattering depth $\lambda_C = (n \sigma_T)^{-1} \approx 1.5 \times 10^9 n_{15}^{-1}$ cm is much smaller than any characteristic size scale of the system, so that most of the fluorescence photons produced in the photoionization precursor will be absorbed within the disk and thus be unobservable. The emission from the shocked region can therefore be represented by pure thermal plasma emission from an optically thick plasma at the temperature of the shocked material. At any given time, we calculate the emission from the shocked material using XSTAR (Kallman & McCray 1982) in a constant-temperature, purely thermal ionization mode (i. e. with very small photoionization parameter).

4. Results

We have done a series of simulations for a variety of parameters representative of both he-merger and collapsar/hypernova disks. In Fig. 6 we show the temporal evolution of the temperature of material behind the shock, resulting sample X-ray spectra at different times after the onset of the shock wave / disk interaction, and the light curve of the Fe K α line luminosity, for a disk with inner radius at $r_{\text{in}} = 10^{13}$ cm, representative for the he-merger case. In those simulations, we have assumed a disk density profile appropriate for a $25 M_{\odot}$ progenitor, and a mass of $1 M_{\odot}$ for the ejected material. The ejecta are assumed to have an initial velocity of 10^9 cm s $^{-1}$, corresponding to a kinetic energy of 10^{51} ergs in the ejecta. The figure shows that, especially in the later, decaying phase, $\gtrsim 2(1+z) \times 10^4$ s after the onset of the shock wave / disk interaction, the thermal X-ray spectrum from the shocked disk material is strongly line dominated and might yield excellent prospects of detection by X-ray telescopes sensitive at $\lesssim 1$ keV.

Tab. 2 illustrates how the maximum Fe K α line luminosity and the decay time constant of the line emission depend on the mass and velocity of the ejecta shock-heating the pre-ejected disk from the $25 M_{\odot}$ progenitor. The time constant t_d is determined by fitting an $\exp[-(t/t_d)^2]$ law to the decaying portion of the iron line light curves. We find that the shock wave / disk interaction expected for the he-merger scenario can very plausibly produce an Fe K α line of apparent quasi-isotropic luminosity $L_{\text{FeK}\alpha} \sim 10^{44}$ ergs s $^{-1}$ maintained over $t_d \lesssim (1+z) \times 10^4$ s after the ejecta begin to interact with the disk.

Fig. 7 shows the temperature evolution, X-ray spectra, and Fe K α light curve for a case representative of a collapsar / hypernova disk, if the system entered the common-envelope phase ~ 100 y before the GRB. The progenitor is assumed to be a $25M_{\odot}$ star. In this case, the disk inner edge is expected to be located at $r_{\text{in}} \sim 10^{15}$ cm. Results of simulations with different ejecta mass and velocity are summarized in Tab. 3. In this case, maximum iron line luminosities in excess of $\sim 10^{42}$ ergs s $^{-1}$ are still possible, while the typical time delay between the GRB and the onset of the GRB is now $\sim (1+z) \times 10^6$ s.

Comparing simulations with identical disk mass and ejecta mass and velocity, but different inner disk radii, we find an approximate scaling law for the maximum Fe K α line luminosity, $L_{\text{FeK}\alpha} \propto r_{\text{in}}^{-1}$.

5. Observational prospects

In the previous section, we found that in both the helium-merger and in the collapsar/hypernova scenarios, a quasi-thermal X-ray flash from the shock-heated disk may result. A critical and yet very uncertain parameter (especially for the collapsar/hypernova scenario) in the model simulations is the inner disk radius, which is primarily determined by the duration of the common-envelope phase prior to the GRB event. In the he-merger scenario, we expect typically $r_{\text{in}} \sim 10^{13}$ cm, while in the collapsar/hypernova scenario, this parameter could have values 10^{14} cm $\lesssim r_{\text{in}} \lesssim 10^{17}$ cm. The onset and decay time scale of the resulting secondary X-ray flash scale as $\Delta t_X \propto r_{\text{in}}$, while the peak X-ray luminosity is approximately $L_{\text{FeK}\alpha} \propto r_{\text{in}}^{-1}$. Since the continuum X-ray afterglows from the (probably beamed) relativistic ejecta typically decay with temporal indices $\chi \gtrsim 1.2$, (if $F_X(t) \propto t^{-\chi}$), detection of the secondary, thermal X-ray outbursts predicted by the he-merger and collapsar/hypernova scenarios might be favored by larger disk radii, as long as the resulting X-ray flux remains above the detection threshold of currently operating X-ray telescopes.

Fig. 8 shows the absorbed 0.1 – 10 keV peak fluxes resulting from two of our simulations, as a function of redshift of the GRB source. Shown are representative cases for $r_{\text{in}} = 10^{13}$ cm and $r_{\text{in}} = 10^{15}$ cm (see also Figs. 6 and 7), corresponding to onset delays of $\sim (1+z) \times 10^4$ s and $\sim (1+z) \times 10^6$ s, respectively. Two

plausible values of the Galactic neutral hydrogen column density, N_H , are used. Given that the nominal point source sensitivity for a 10 ksec exposure on *Chandra*'s ACIS detectors is $\sim 4 \times 10^{-15}$ ergs cm^{-2} s^{-1} , while for the EPIC detectors on board *XMM-Newton* this limit is $\sim 10^{-14}$ ergs cm^{-2} s^{-1} , the predicted X-ray flashes from the shock wave / disk interaction may be detectable out to redshifts of at least $z \sim 1$ for an inner disk radius of $r_{\text{in}} \sim 10^{15}$ cm. For a source at $z = 1$ with $r_{\text{in}} = 10^{15}$ cm, we would expect the onset of the secondary X-ray burst ~ 3 weeks after the GRB.

6. Summary

During the progenitor evolution of collapsar/hypernova and he-merger GRBs, a hydrogen disk is formed around the central engine. These GRB engines produce a jet along the disk axis, and the relativistic outburst which produces the gamma-rays does not interact with this disk. However, both of these engines are likely to expel $\gtrsim 1 M_\odot$ along the equator at lower velocities ($\sim 10^9$ cm s^{-1}). The interaction of the explosion ejecta with the expelled disk may produce X-ray luminosities in excess of $\sim 10^{44} (r_{\text{in}}/10^{13} \text{ cm})^{-1}$ ergs s^{-1} with a delay of $\sim (r_{\text{in}}/10^{13} \text{ cm}) (1 + z) \times 10^4$ s after the GRB. For gamma-ray bursts with a redshift $z \lesssim 1$, this emission is well within the capabilities of the latest X-ray satellites (e.g. *Chandra* and *XMM-Newton*). Thus, long-term monitoring of X-ray afterglows over several weeks after the GRB (most notably, even after the direct afterglow radiation has faded to undetectable levels) may lead to the detection of these secondary X-ray flashes which would yield valuable information about the nature and pre-burst evolution of the GRB progenitor.

The work of M.B. is supported by NASA through Chandra Postdoctoral Fellowship Award Number PF 9-10007, issued by the Chandra X-ray Center, which is operated by the Smithsonian Astrophysical Observatory for and on behalf of NASA under contract NAS 8-39073. C.L.F was supported by a Feynman Fellowship at LANL, NSF (AST-97-31569), and the US DOE ASCI Program (W-7405-ENG-48). It is a pleasure to thank P. Pinto for helpful advice and discussions.

REFERENCES

- Arnaud, M., & Raymond, J. C., 1992, ApJ, 398, 394
- Böttcher, M., Dermer, C.D., Crider, A.W., & Liang, E.P. 1999, A&A, 343, 111
- Böttcher, M., Dermer, C.D., & Liang, E.P. 1999, A&AS, 138, 543
- Böttcher, M. 2000, ApJ, 539, 102
- Bulik, T., & Belczyński, K., in Proc. of the 5th Huntsville Symposium on Gamma-Ray Bursts, ed. R. M. Kippen, R. S. Mallozzi, & G. J. Fishman, AIP Conf. Proc. 526, 648
- Collins, T.J.B., Frank, A., Bjorkman, J.E., Livio, M. 1999, ApJ, 512, 322
- Fryer, C. L., & Woosley, S. E. 1998, ApJ, 501, 780
- Fryer, C.L., Kalogera, V., submitted to ApJ, astro-ph/9911312
- Fryer, C.L., Woosley, S.E., & Hartmann, D.H., 1999, ApJ, 526, 152

- Ghisellini, G., Haardt, F., Campana, S., Lazzati, D., Covino, S., 1999, *ApJ*, 517, 168
- Israelian, G., Rebolo, R., Basri, G., Casares, J., Martin, E.L. 1999, *Nature*, 401, 142
- Kallman, T. R., & McCray, R., 1982, *ApJS*, 50, 263
- Lazzati, D., Campana, S., Ghisellini, G. 1999, *MNRAS*, 304, L31
- MacFadyen, A.I., & Woosley, S.E. 1999, *ApJ*, 524, 262
- Paerels, F., Kuulkers, E., Heise, J., & Liedahl, D. A., 2000, *ApJ*, 535, L25
- Piro, L., et al., 1999, *ApJ*, 514, L73
- Podsiadlowski, P. 1992, 104, 717
- Raymond, J., C., & Smith, B. W., 1977, *ApJS*, 35, 419
- Ruffert, M., Janka, H.-T., & Schaefer, G. 1996, *A&A*, 311, 532
- Rybicki, G. B., & Lightman, A. P., 1979, “Radiative Processes in Astrophysics”, John Wiley & Sons
- Sandquist, E., Taam, R.E., Chen, X., Bodenheimer, P., & Burkert, A. 1998, *ApJ*, 500, 909
- Schaerer, D., Charbonnel, C., Meynet, G., Maeder, A., Schaller, G. 1993, *A&AS*, 102, 339
- Stella, L., & Vietri, M. 1998, *ApJ*, 507, L45
- van Regemorter, H., 1962, *ApJ*, 136, 906
- Vietri, M., Perola, C., Piro, L., & Stella, L. 1999, *MNRAS*, 308, L29
- Wellstein, S., & Langer, N. 1999, *A&A*, 350, 148
- Weth, C., et al. 2000, *ApJ*, 534, 581
- Woosley, S.E., Weaver, T.A. 1995, *ApJS*, 101, 181
- Zhang, W., & Fryer, C.L., 2000, in preparation

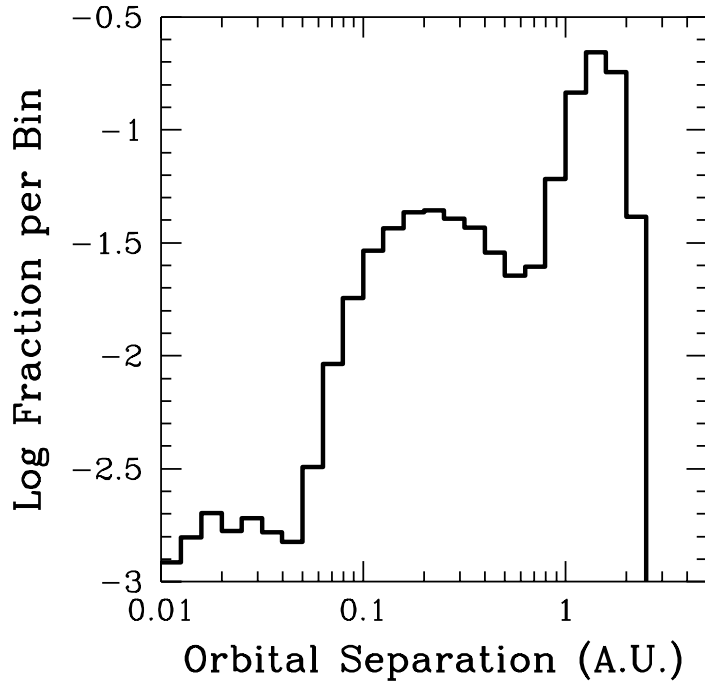


Fig. 1.— Distribution of orbital separations for he-mergers just prior to the common envelope phase, plotted as the fraction per bin (orbital separation is logarithmically spaced). There are two peaks, one at 0.2 astronomical units, and the other at roughly 1.5 astronomical units.

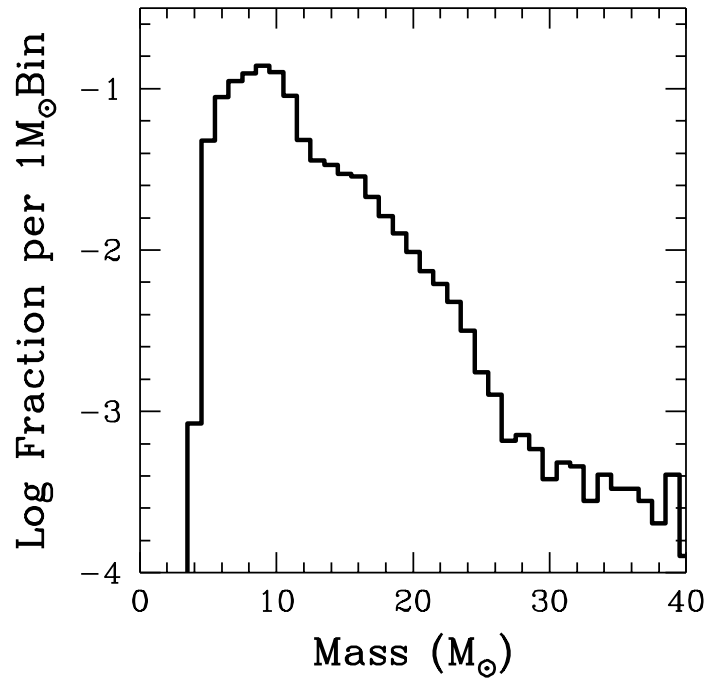


Fig. 2.— Distribution of companion masses for helium mergers. Although the peak is at $9 M_{\odot}$, it is likely that the more massive companions will produce more luminous bursts (their larger helium cores provide more fuel for the GRB).

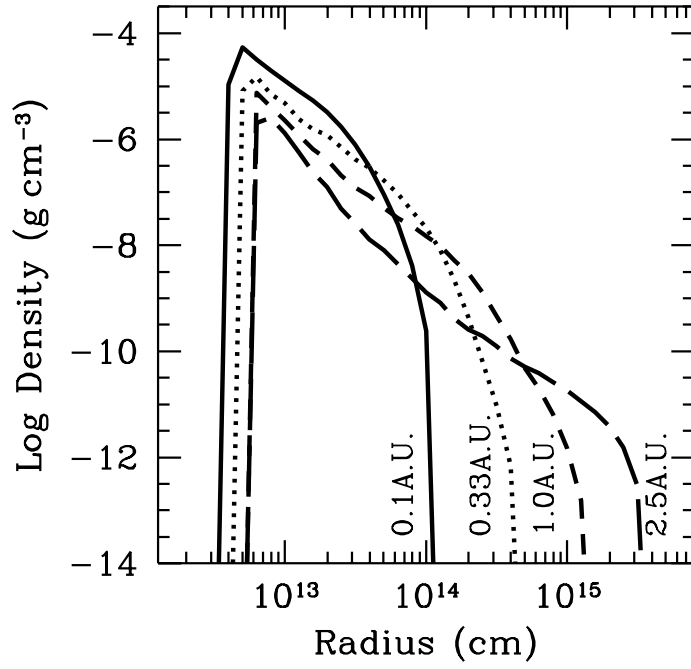


Fig. 3.— Density vs. radius of the hydrogen disk formed during inspiral of a neutron star into a $15 M_{\odot}$ star (Heger 1999) as it expands off the main sequence for a range of binary separations: 0.1, 0.33, 1, 2.5 A.U. We assume the star engulfs its compact companion when its radius exceeds the orbital separation.

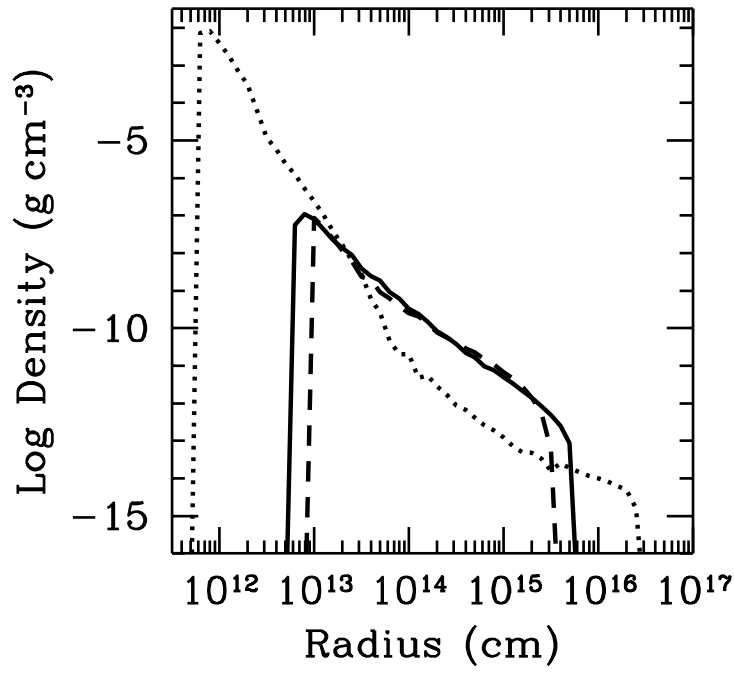


Fig. 4.— Density vs. radius of the hydrogen disk formed during inspiral of a neutron star into 15, 25, and 40 M_{\odot} pre-collapse stars (Woosley & Weaver 1995). The density profiles of these pre-collapse models give a good estimate of the structure of these stars after helium ignition (Case C mass transfer).

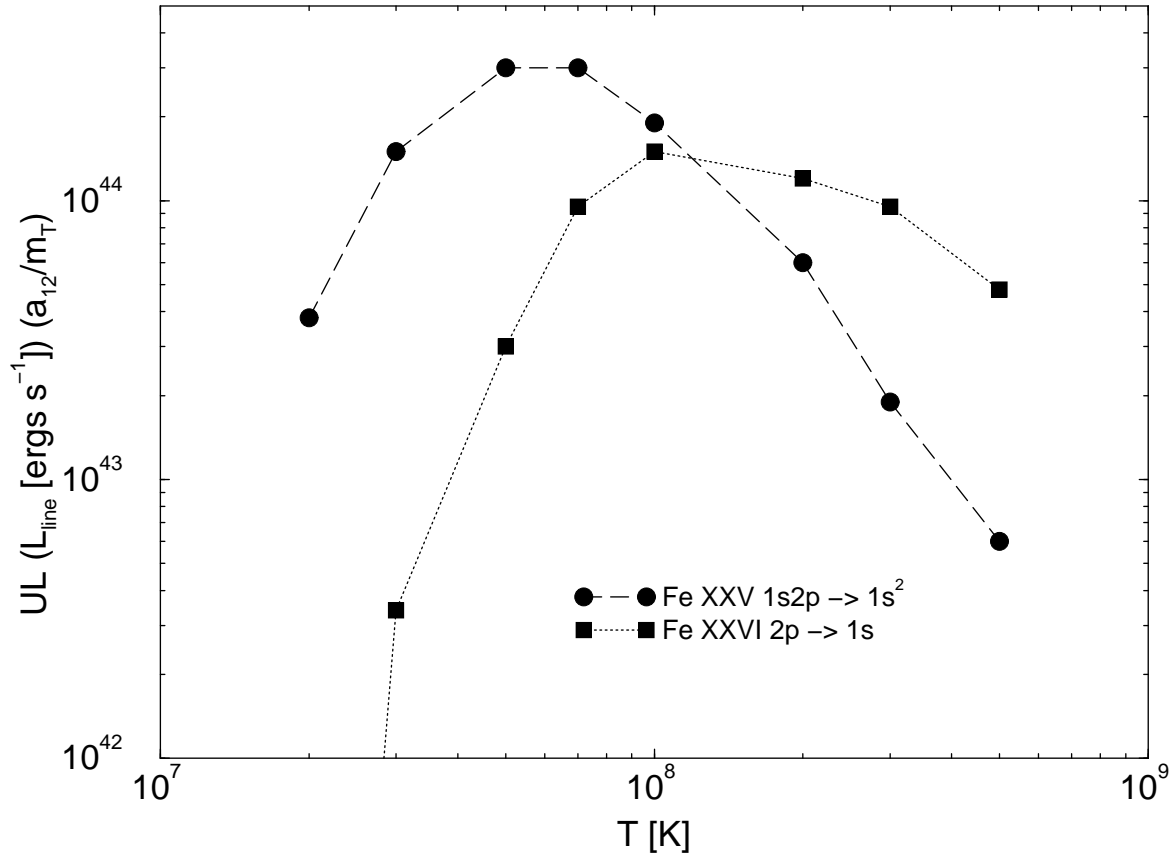


Fig. 5.— Estimated upper limits on the luminosity in the Fe XXV He α ($1s2s \rightarrow 1s^2$) and Fe XXVI H α ($2p \rightarrow 1s$) lines at ~ 6.7 keV from a hot, thermal torus at $r = 10^{13} r_{13}$ cm, as a function of temperature of the torus material.

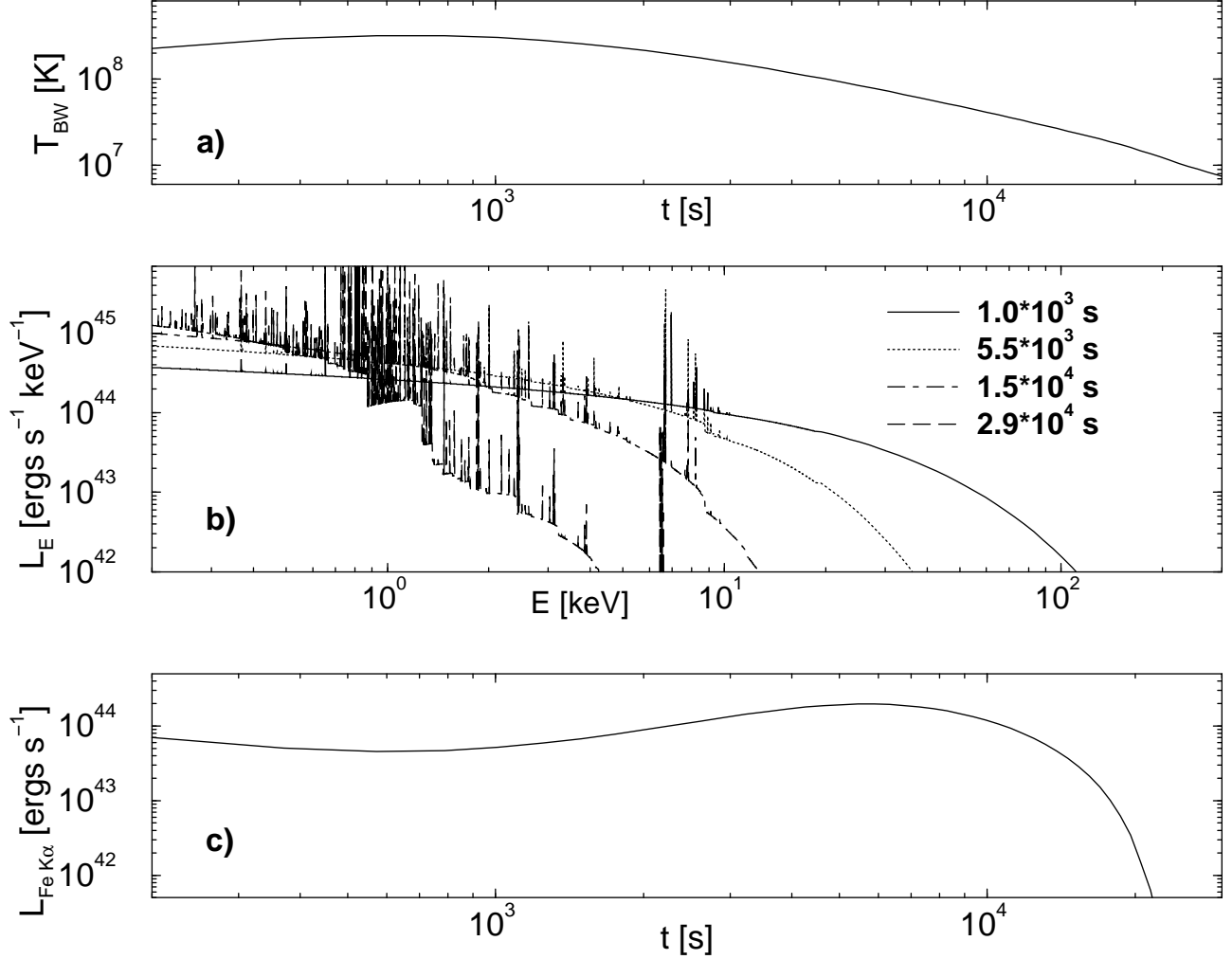


Fig. 6.— Temporal evolution of the temperature (top panel), X-ray spectra (middle panel), and light curve of the emission in the Fe K α line (bottom panel) for $1 M_{\odot}$ ejected at 10^9 cm s $^{-1}$ and interacting with the disk of pre-ejected material from a $25 M_{\odot}$ progenitor with disk inner radius $r_{\text{in}} = 10^{13}$ cm. $t = 0$ corresponds to the time of the onset of the blast-wave/disk interaction, i. e. $(1+z)r_{\text{in}}/v_s \sim (1+z) \times 10^4$ s after the GRB/supernova explosion. All times and photon energies quoted in the figure refer to the cosmological rest frame of the GRB source.

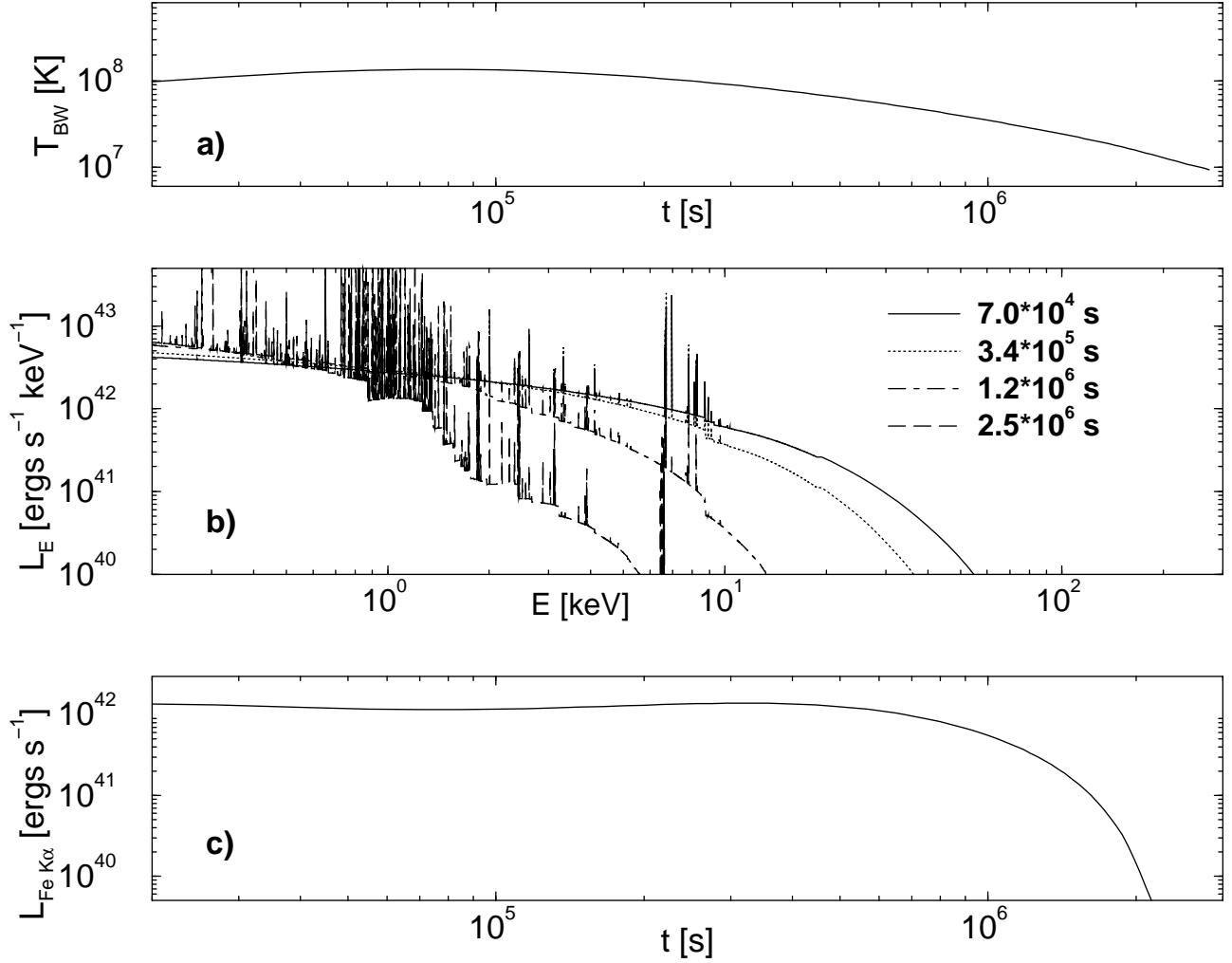


Fig. 7.— Same as Fig. 6, except for disk inner radius, $r_{\text{in}} = 10^{15}$ cm. Thus, here $t = 0$ corresponds to $\sim (1+z) \times 10^6$ s after the GRB/supernova explosion.

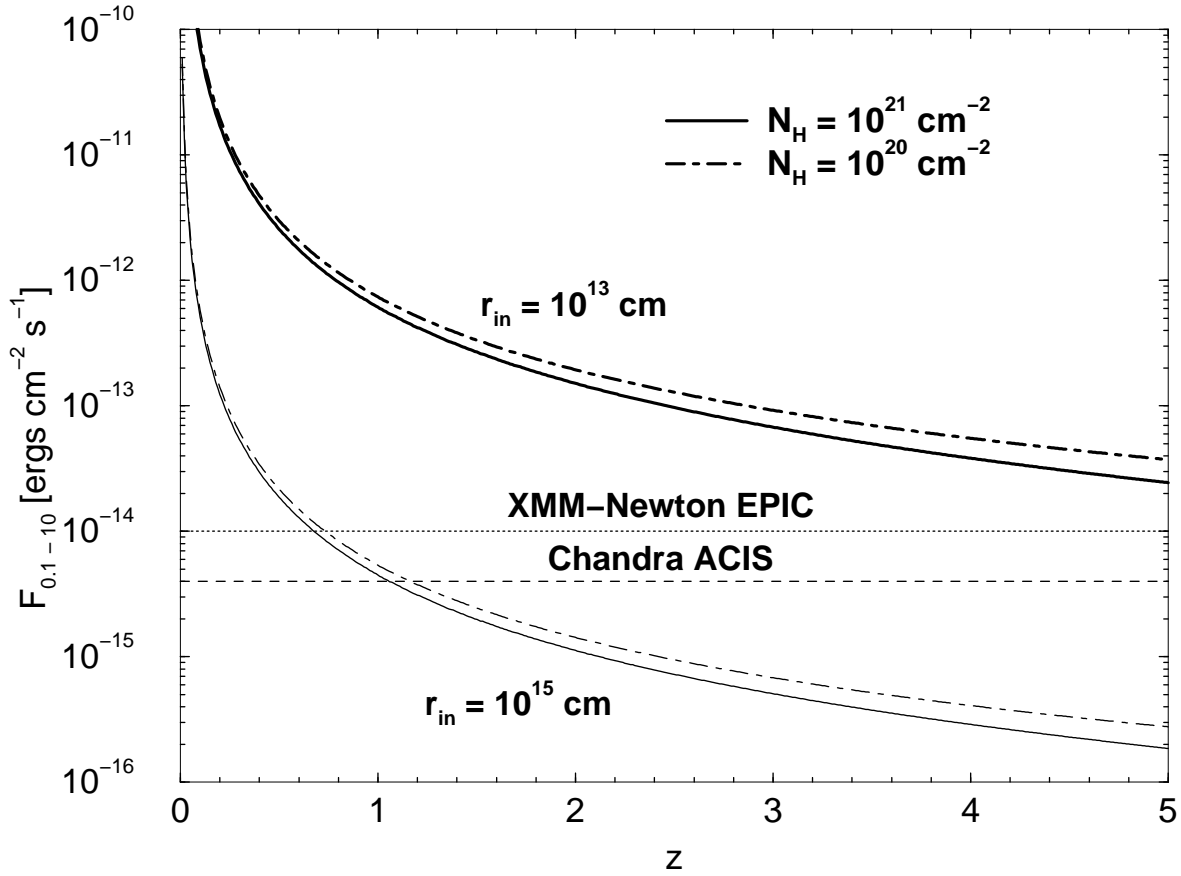


Fig. 8.— Peak 0.1 – 10 keV X-ray fluxes, accounting for Galactic absorption, as a function of redshift, for the blast wave simulations illustrated in Fig. 6 (thick lines) and Fig. 7 (thin lines). Horizontal lines show the nominal, estimated sensitivity limits of the *Chandra* ACIS and *XMM-Newton* EPIC detectors, respectively, for a 10 ksec exposure.

Table 1. Emissivity parameters x , and upper limits on the resulting luminosity in the ~ 6.7 keV iron lines of Fe XXV and Fe XXVI from a hot thermal torus.

T [K]	$x_{\text{He}\alpha}$	$\frac{\text{UL}(L_{\text{He}\alpha}) a_{12}}{m_{\text{T}}} [\text{ergs s}^{-1}]$	$x_{\text{H}\alpha}$	$\frac{\text{UL}(L_{\text{H}\alpha}) a_{12}}{m_{\text{T}}} [\text{ergs s}^{-1}]$
2×10^7	2.2	3.8×10^{43}	7.0	6.0×10^{38}
3×10^7	1.6	1.5×10^{44}	3.4	2.4×10^{42}
5×10^7	1.3	3.0×10^{44}	2.3	3.0×10^{43}
7×10^7	1.3	3.0×10^{44}	1.8	9.5×10^{43}
1×10^8	1.5	1.9×10^{44}	1.6	1.5×10^{44}
2×10^8	2.0	6.0×10^{43}	1.7	1.2×10^{44}
3×10^8	2.5	1.9×10^{43}	1.8	9.5×10^{43}
5×10^8	3.0	6.0×10^{42}	2.1	4.8×10^{43}

Table 2. Simulated maximum quasi-isotropic Fe $K\alpha$ line luminosities and decay time scales t_d for ejecta of different mass and velocities shock-heating the pre-ejected disk from a $25 M_{\odot}$ progenitor, $r_{\text{in}} = 10^{13}$ cm.

v_{ej} [10^9 cm s $^{-1}$]	M_{ej} [M_{\odot}]	E_{ej} [10^{51} ergs]	$L_{K\alpha}(t_{\text{max}})$ [10^{43} ergs s $^{-1}$]	t_d [10^3 s]
1	0.5	0.5	14	11
1	1	1	18	12
1	2	2	29	13
0.707	1	0.5	16	9.5
1.414	1	2	20	16
0.707	0.5	0.25	11	8.5
0.5	0.5	0.125	9.1	7.0

Table 3. Simulated maximum quasi-isotropic Fe K α line luminosities and decay time scales t_d for ejecta of different mass and velocities shock-heating the pre-ejected disk from a $25 M_\odot$ progenitor, $r_{\text{in}} = 10^{15}$ cm.

v_{ej} [10^9 cm s $^{-1}$]	M_{ej} [M_\odot]	E_{ej} [10^{51} ergs]	$L_{\text{K}\alpha}(t_{\text{max}})$ [10^{41} ergs s $^{-1}$]	t_d [10^5 s]
1	0.5	0.5	8.7	8.0
1	1	1	14	9.0
1	2	2	27	9.0
0.707	1	0.5	13	6.5
1.414	1	2	13	12
0.707	0.5	0.25	8.0	6.5